Comparison of Oxygen Permeability and Stability of Perovskite Type $La_{0.2}A_{0.8}Co_{0.2}Fe_{0.8}O_{3-\delta}$ (A = Sr, Ba, Ca) Membranes

Shiguang Li, Wanqin Jin, Pei Huang, Nanping Xu,* and Jun Shi

Membrane Science & Technology Research Center, Nanjing University of Chemical Technology, Nanjing 210009, P. R. China

Y. S. Lin

Department of Chemical Engineering, University of Cincinnati, Cincinnati, Ohio 45221-0171

Michael Z.-C. Hu† and E. Andrew Payzant‡

Chemical Technology Division, Metals & Ceramics Division, Oak Ridge National Laboratory, Oak Ridge, Tennessee 37831-6224

The oxygen permeation and stability of $La_{0.2}A_{0.8}Co_{0.2}Fe_{0.8}O_{3-\delta}$ (A = Sr, Ba, Ca) perovskite-type membranes were studied at high temperatures and low oxygen partial pressures. The oxygen vacancy diffusivity and concentration gradient calculated from the unsteady-state and steady-state oxygen data for the three membranes decrease in the order of Sr > Ba > Ca. The activation energies for oxygen permeation increase in the order of Sr < Ba < Ca. The oxygen permeation data of the three membranes can be explained by the average bond energy, free volume, and critical radius of the materials. After exposure to air at 1173 K for 10 h, part of $La_{0.2}Sr_{0.8}Co_{0.2}Fe_{0.8}O_{3-\delta}$ transforms to La_2O_3, SrO, CoO, and Fe and the crystallite size of the perovskite phase decreases. These changes were not observed for $La_{0.2}Ba_{0.8}Co_{0.2}Fe_{0.8}O_{3-\delta}$ under the same conditions, indicating that $La_{0.2}Ba_{0.8}Co_{0.2}Fe_{0.8}O_{3-\delta}$ membrane is much more stable than $La_{0.2}Sr_{0.8}Co_{0.2}Fe_{0.8}O_{3-\delta}$ at high temperatures and low oxygen partial pressures.

1. Introduction

Mixed conducting membranes that exhibit high oxygen ionic and electronic conductivities gained great interest as clean, efficient, and economical means of producing oxygen from air or other oxygen-containing gas mixtures. They will be most competitive at small and intermediate-scale levels in which flexibility of operation is desired, and may eventually challenge the present commercial status of cryogenics, pressure-swing adsorption, and polymeric membranes.[1−4] Another application of mixed-conducting oxide membranes is found in the field of chemical processing, including the partial oxidation of light hydrocarbons, e.g. conversion of natural gas to value-added products such as ethane/ethene [5−10] and syngas.[11−16]

Among mixed conducting oxides, materials with oxygen-deficient perovskite (ABO_3) and perovskite-related structures have received much attention for numerous applications.[17−26] Teraoka et al.[27] were the first to report very high oxygen fluxes through the A-site substitution compositions, $La_{0.6}A_{0.4}Co_{0.8}Fe_{0.2}O_{3-\delta}$ (A = Sr, Ba, Ca) series oxides, which become highly defective at elevated temperatures and reduced oxygen partial pressure. Stevenson et al.[28] and Tsai et al.[13] also have studied oxygen permeability of A-site substitution perovskite-type oxides. Their work focused on $La_{0.4}A_{0.6}Co_{0.2}Fe_{0.8}O_{3-\delta}$ (A = Sr, Ba, Ca) oxides system. A comparison of oxygen permeation properties of $La_xA_{1-x}Co_yFe_{1-y}O_{3-\delta}$ (A = Sr, Ba, Ca; x = 0.2, 0.4, 0.6; y = 0.8, 0.6, 0.4) reported by these researchers is shown in Table 1.

As shown in Table 1, in the study of Teraoka et al.[27] the oxygen permeation flux of A-site substitution decreases in the order, Ba > Ca > Sr. The results of Tsai et al.[13] agree with those of Teraoka et al.,[27] But Stevenson et al.[28] obtained the different results with the oxygen permeation fluxes decreasing in the order Sr > Ba > Ca. Such conflicting results reflect the difficulties in measuring the oxygen fluxes at high temperature, and possible effects of different preparation methods on the oxygen permeability of the perovskite-type membranes.

Although the oxygen flux tends to be highest in materials having high A-site substitution, other factors need to be considered. In particular, the substitution of Sr for the respective La decreases the high-temperature phase stability in the low oxygen partial pressure environment. One of the typical examples is $SrCo_{0.8}Fe_{0.2}O_{3-\delta}$, which has a high reported oxygen permeation rate, 3.1 cm^3 (STP)·min^{-1} cm^{-2} (temperature, 1123 K; membrane thickness, 1 mm),[29] but has both an abrupt first-order phase transition at about 1063 K[30] and a susceptibility to reduction in the reducing atmospheres.[14]

The purpose of this study was to investigate further the oxygen permeability and stability of A-site substitution, $La_{0.2}A_{0.8}Co_{0.2}Fe_{0.8}O_{3-\delta}$ (A = Sr, Ba, Ca), perovskite-type membranes. Oxygen vacancy diffusivity and oxygen vacancy concentration, activation energy, average bonding energy, free volume and critical radii of the A-site substitution perovskite-type oxides were calculated and used to explain the different oxygen permeation fluxes. The membrane stability was also studied

* Corresponding author. Tel: 0086-025-3319580; Fax: 0086-025-3300345; E-mail: npxu@dns.njuct. edu. cn.

† Chemical Technology Division.

‡ Metals & Ceramics Division.

10.1021/ie9900014 CCC: $18.00
Published on Web 07/15/1999

Table 1. Comparison of Oxygen Permeation Properties of $La_xA_{1-x}Co_yFe_{1-y}O_{3-\delta}$ (A = Sr, Ba, Ca; x = 0.2, 0.4. 0.6; y = 0.8, 0.6, 0.4) Reported in Literatures

studies	powder synthesis	membrane	thickness (cm)	J_{O_2} (900 °C) (cm^3/cm^2 min)	E_a (kJ/mol)
Teraoka (1988)	solid-state reaction	$La_{0.6}Sr_{0.4}Co_{0.8}Fe_{0.2}O_{3-\delta}$	0.2	0.62	86.3
		$La_{0.6}Ba_{0.4}Co_{0.8}Fe_{0.2}O_{3-\delta}$	0.2	2.11	57.2
		$La_{0.6}Ca_{0.4}Co_{0.8}Fe_{0.2}O_{3-\delta}$	0.2	1.80	75.0
Tsai (1998)	modified citrate pyrolysis	$La_{0.4}Sr_{0.6}Co_{0.2}Fe_{0.8}O_{3-\delta}$	0.055	0.11	105.6
		$La_{0.4}Ba_{0.6}Co_{0.2}Fe_{0.8}O_{3-\delta}$	0.055	0.72	72.4
		$La_{0.4}Ca_{0.6}Co_{0.2}Fe_{0.8}O_{3-\delta}$	0.055	0.19	95.3
Stevenson (1996)	glycine-nitrate combustion	$La_{0.4}Sr_{0.6}Co_{0.2}Fe_{0.8}O_{3-\delta}$	0.2	0.55	91.7
		$La_{0.4}Ba_{0.6}Co_{0.2}Fe_{0.8}O_{3-\delta}$	0.2	0.45	86.8
		$La_{0.4}Ca_{0.6}Co_{0.2}Fe_{0.8}O_{3-\delta}$	0.2	0.07	67.5
		$La_{0.2}Sr_{0.8}Co_{0.2}Fe_{0.8}O_{3-\delta}$	0.2	0.68	82.0
		$La_{0.2}Ba_{0.8}Co_{0.2}Fe_{0.8}O_{3-\delta}$	0.2	0.42	62.7

by an in situ high-temperature X-ray diffraction (HTXRD) in air and argon atmosphere.

2. Experimental Section

2.1. Powder and Membrane Preparation. Compositions with the system $La_{0.2}A_{0.8}Co_{0.2}Fe_{0.8}O_{3-\delta}$ (A = Sr, Ba, Ca) were synthesized by solid-state reaction of the constituent cationic salts (the Second Chemical Industry of Shanghai, purity of 99.9%). In the preparation of the oxides, appropriate amounts of La_2O_3, $Sr(CO_3)_2$ (or $Ba(CO_3)_2$ $Ca(CO_3)_2$), Co_2O_3, Fe_2O_3 were mixed and ball-milled in pure water for 24 h. After being dried at 353 K for 24 h, the mixture was ground and sintered in air at 1173 K for 5 h. The heating and cooling rates were controlled at 2 K/min. The sintered powder was sifted to an average particle size of about 8 μm.

The membranes were prepared by isostatic pressing. A die was used for the shape-forming process, which includes loading, pressing, and ejecting. A total of 12 tons of oil pressure was applied on the plunger of the die by the press, which resulted in a pressure of 400 MPa on the powders. After 5 min, the pressure was released and the die was removed from the press. Results showed that 1−2 g of powder produced a 1- to 2-mm-thick, 16-mm-diameter green disk. The green disks of LSCF were sintered in air at 1523 K for 10 h. The heating and cooling rates were controlled at 2 K/min.

2.2. Powder and Membrane Characterization. The crystal structures of the resulting membranes were determined by an in situ HTXRD analysis using Cu Kα radiation (PAD X, Scintag Inc.). Each sample was tested at several temperatures in oxygen-rich atmosphere (in air) and oxygen-lean atmosphere (in argon) using a Pt holder. The heating rate was 4 K/min, and the sample was stabilized at every temperature for 1 h. A range of diffraction angles from 20° to 90° were used. Data collection was accomplished using DMSNT software (Scintag Inc., Cupertino, CA), and data analysis was undertaken using Jade software (Materials Data Inc., Livermore, CA).

Thermogravimetric analysis (TGA, model SDT2960) was performed on powder specimens from room temperature to 1573 K using a heating and cooling rate of 5 K/min. Buoyancy corrections were performed using a platinum standard. The TGA measurements were performed in air and N_2 atmosphere.

The membrane surface morphology was examined by high-resolution scanning electron microscopy (HR−SEM) (JEOL JSM-6300). Surface element analysis of the membranes was performed by energy dispersive spectroscopy (EDS) (U. S. Kevex-Sigma). The densities of the sintered membranes were determined by the Archimedes method. These densities exceeded 90% of the theoretical one in all cases.

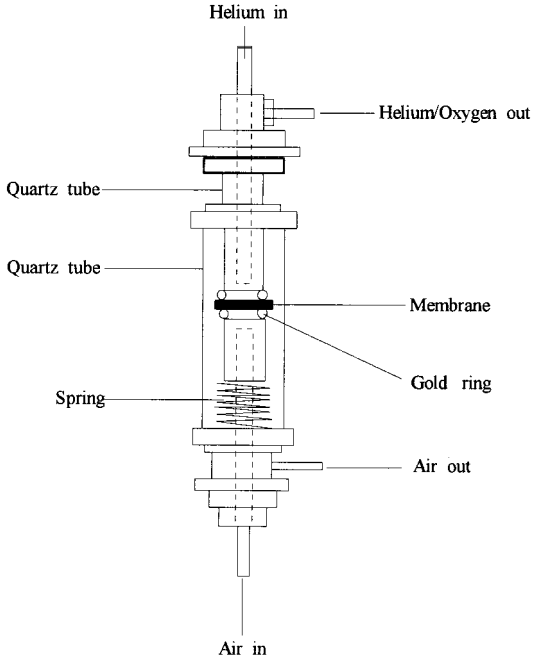

Figure 1. Schematic of high temperature oxygen permeation module.

2.3. Oxygen Permeation Measurement. The membrane permeation module used in this work is shown in Figure 1. A sintered membrane disk was polished to the thickness of interest and then mounted on a quartz tube using a gold ring seal. A pressure of approximately 0.1 MN/m^2 was applied by releasing a spring from the bottom of the ring to provide close contact for quartz/gold/membrane joints while the temperature was controlled at 1293 K for 10 h. A tubular furnace whose temperature could be controlled with ±1 K by a microprocessor (model AI-708PA, Xiamen Yuguang Electronics Technology Research Institute, China) was used for heating. A heating rate of 1.5 K/min was used to form the bonding. The furnace was then cooled to the temperature of interest at a 1.5 K/min cooling rate. Experimental results showed that the airtight sealing could be sustained at temperatures from 473 to 1273 K and pressure drops up to 0.02 MPa between permeate and retentive sides, depending on the strength of the perovskite-type membranes.

In oxygen permeation experiments, the flow rates of the inlet gases were controlled by mass flow controllers (models D07-7A/ZM, Beijing Jianzhong Machine Factory, China). Air was introduced into the upstream of

Table 2. Perovskite Membranes

membrane	thickness (cm)	crystal structure	lattice parameter (Å)	theoretical density (g/cm^3)	sintered density (g/cm^3)
$La_{0.2}Sr_{0.8}$ $Co_{0.2}Fe_{0.8}O_{3-\delta}$	0.2	cubic	3.820	6.03	5.48
$La_{0.2}Ba_{0.8}Co_{0.2}Fe_{0.8}O_{3-\delta}$	0.2	cubic	3.875	6.91	6.36
$La_{0.2}Ca_{0.8}Co_{0.2}Fe_{0.8}O_{3-\delta}$	0.1	cubic	3.780	5.05	4.85

the membrane. Helium as the sweep gas for the permeating oxygen was fed to the downstream of the membrane. Both upstream and downstream were maintained at the atmospheric pressure. The effluent streams were analyzed by gas chromatography (model Shimabzu GC-7A), which was equipped with a 2 m 5 Å molecular sieve operated at 40 °C, with H_2 as the carrier gas. The oxygen permeation flow through the membrane was calculated from the flow rates and the oxygen concentrations of the effluents. Details of the schematic of the oxygen permeation system was reported in previous publications.[33,34]

3. Results and Discussion

3.1. Perovskite-Type Powder and Membrane. Perovskite-type powders synthesized in this study are summarized in Table 2. Lattice parameters and theoretical densities (shown in Table 2), were calculated from the X-ray powder patterns. The relatively lower sintered density might be caused by the closed porosity, which can be seen by high-resolution scanning electron microscopy. The closed porosity might be caused by the grain growth or by air trapped during the pressing. However, measurement of the nitrogen permeation rate confirmed that open porosity did not exist.

3.2. Oxygen Permeation. Figure 2 shows oxygen permeation flux for $La_{0.2}A_{0.8}Co_{0.2}Fe_{0.8}O_{3-\delta}$ (A = Sr, Ba, Ca) membranes as a function of time after the downstream was shifted from air to helium (upstream was air). The oxygen permeation flux, starting at a much higher value, decreases with time and eventually levels off. Such unsteady steady oxygen permeation flux after the start of permeation measurements was reported by several groups.[12,30−34] Zeng et al.[31] pointed out that the excessive amount of the oxygen permeated from the membrane before the steady state equaled the difference of the oxygen in the membrane between the steady state of oxygen permeation and initial state before permeation. During this unsteady-state process, the oxygen vacancy concentration C_v and oxygen permeation flux J_{O_2} can be obtained[34]:

$$C_v = C_v' + (C_v'' - C_v')\frac{x}{L} + \sum_{1}^{\infty} \sin\frac{n\pi x}{L} \exp(-D_v n^2\pi^2 t/L^2) \times \frac{2\cos n\pi}{n\pi}(C_v' - C_v'') \quad (1)$$

$$J_{O_2} = \frac{D_v(C_v'' - C_v')}{2L}[1 + \sum_{1}^{\infty} 2\exp(-D_v n^2\pi^2 t/L^2)] \quad (2)$$

where C and D are the concentration and diffusivity of a charged species with subscripts v indicating the oxygen vacancy; superscripts ′ and ″ represent the upstream and downstream membrane interfaces, L is the membrane thickness, and t is the time.

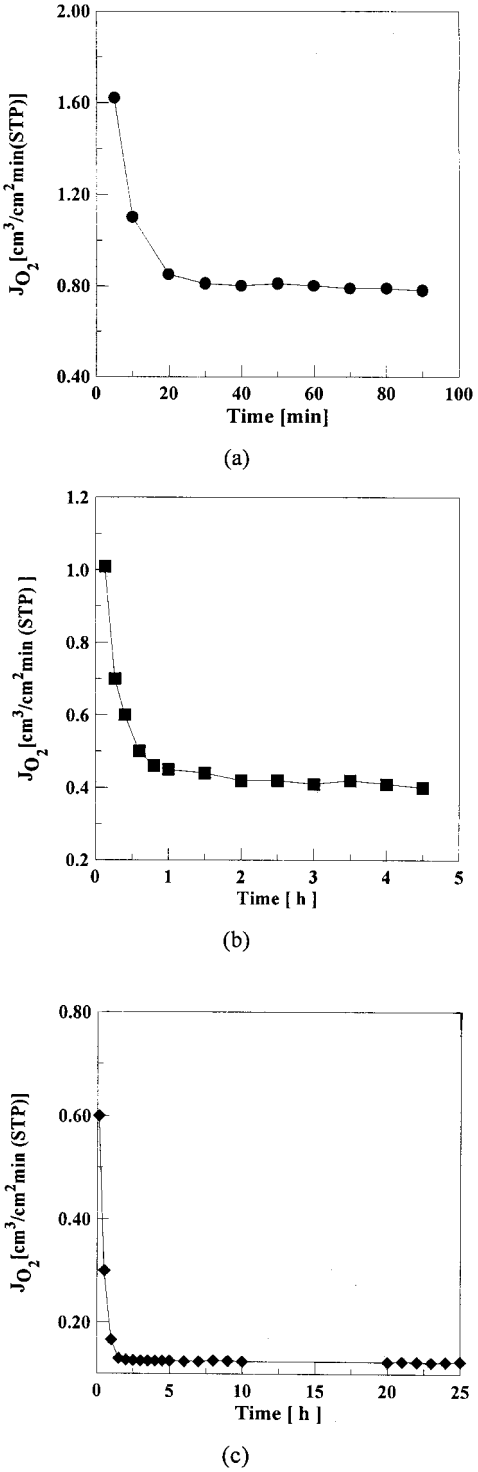

Figure 2. Transient process of oxygen permeation through perovskite-type membranes at 1173 K and the partial pressure of $0.21/1 \times 10^{-3}$ atm (helium flow rate, 30 mL/min.): (a) $La_{0.2}Sr_{0.8}Co_{0.2}Fe_{0.8}O_{3-\delta}$; (b) $La_{0.2}Ba_{0.8}Co_{0.2}Fe_{0.8}O_{3-\delta}$; (c) $La_{0.2}Ca_{0.8}Co_{0.2}Fe_{0.8}O_{3-\delta}$.

Equation 2 indicates that the measured oxygen flux includes two parts: the time-independent, steady-state contribution; and a time-dependent contribution due to the loss of the oxygen in the membrane material.

Table 3. Oxygen Permeation Properties of Perovskite Membranes

membrane	equilibration time (min)	steady state J_{O_2} (950 °C)[a] (cm^3/cm^2 min)	E_a (kJ/mol)	D_v (cm^2/s)
$La_{0.2}Sr_{0.8}Co_{0.2}Fe_{0.8}O_{3-\delta}$	20	0.81	106.0	1.71×10^{-5}
$La_{0.2}Ba_{0.8}Co_{0.2}Fe_{0.8}O_{3-\delta}$	40	0.40	123.3	8.54×10^{-6}
$La_{0.2}Ca_{0.8}\ Co_{0.2}Fe_{0.8}O_{3-\delta}$	120	0.12	144.0	2.85×10^{-6}

[a] Oxygen partial pressure, $0.21/1 \times 10^{-3}$ atm; helium flow rate, 30 mL/min.

Equation 2 shows that when $t = 0$, $J_{O_2} \rightarrow \infty$. Thus, initially very large oxygen permeation flux could be observed. The permeation flux decreases with time, with the rate depending on the diffusivity of the oxygen vancancy and membrane thickness, as shown by eq 2. Equation 2 also shows that when $t \rightarrow \infty$, the oxygen permeation flux at steady state can be obtained:

$$J_{O_2} = \frac{D_v(C_v'' - C_v')}{2L} \tag{3}$$

which is consistent with the results of Zeng et al.[31]

Although theoretically it takes an infinite time for oxygen permeation flux to reach the steady state, practically we can define that the steady state is reached when the actual permeation flux is about 1% larger or smaller than the steady-state value. The equilibrium time t_{equil} can be measured experimentally. Then the diffusivity can be calculated from eq 2 by:

$$[\sum_{1}^{\infty} 2 \exp(-D_v n^2 \pi^2 t_{equil}/L^2)] = 0.01 \tag{4}$$

Table 3 gives the equilibration time, the oxygen permeation flux at the steady state, and the calculated diffusivity. As listed in Table 3, the oxygen permeation flux and diffusivity for the perovskite-type membranes with A-site substitution decrease in the order: Sr > Ba > Ca, which agrees with the study of Stevenson et al.,[28] but is different from those of Teraoka et al.[27] and Tsai et al.[13]

The oxygen vacancy concentration difference (ΔC_v) (or oxygen vacancy gradient, $\Delta C_v/L$) of the membranes can be calculated from eq 3, because the oxygen permeation flux at the steady-state and oxygen vacancy diffusivity are known. TGA is the other method to determine ΔC_v, Figure 3a and 3b shows TGA results of $La_{0.2}A_{0.8}Co_{0.2}Fe_{0.8}O_{3-\delta}$ (A = Sr, Ba, Ca) membranes in air atmosphere and in N_2 atmosphere (oxygen partial pressure of 1×10^{-3} atm). Values of δ and ΔC_v of $La_{0.2}A_{0.8}Co_{0.2}Fe_{0.8}O_{3-\delta}$ (A = Sr, Ba, Ca) membranes at different temperatures can be obtained from the figure, assuming that δ is the same at room temperature in air and N_2 atmospheres. ΔC_v is related to δ by:

$$\Delta C_v = \frac{\delta_{N_2} - \delta_{air}}{V_m} \tag{5}$$

where δ_{N_2} and δ_{air} are δ at air atmosphere and N_2 atmosphere, respectively. V_m is the molar volume of the membrane.

For $La_{0.2}Sr_{0.8}Co_{0.2}Fe_{0.8}O_{3-\delta}$ and $La_{0.2}Ba_{0.8}Co_{0.2}Fe_{0.8}O_{3-\delta}$ membranes, values of ΔC_v obtained by the two methods at the temperature of 1223 K are very similar. There is a small difference for $La_{0.2}Ca_{0.8}Co_{0.2}Fe_{0.8}O_{3-\delta}$ membrane probably because the oxygen permeation of $La_{0.2}Ca_{0.8}Co_{0.2}Fe_{0.8}O_{3-\delta}$ membrane was low and the equilibrium time of this membrane was difficult to determine accurately. The resulting oxygen vacancy concentration differences of $La_{0.2}Sr_{0.8}Co_{0.2}Fe_{0.8}O_{3-\delta}$ and $La_{0.2}Ba_{0.8}Co_{0.2}Fe_{0.8}O_{3-\delta}$ membranes are very similar and higher than that of $La_{0.2}Ca_{0.8}Co_{0.2}Fe_{0.8}O_{3-\delta}$ membrane.

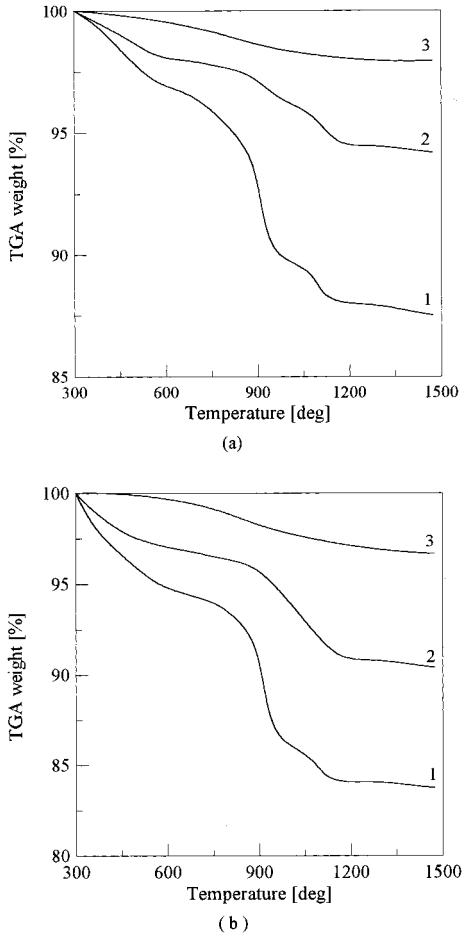

Figure 3. TGA results of $La_{0.2}A_{0.8}Co_{0.2}Fe_{0.8}O_{3-\delta}$ (A = Sr, Ba, Ca) membranes: (a) in air atmosphere; (b) in N_2 atmosphere; (1) $La_{0.2}Sr_{0.8}Co_{0.2}Fe_{0.8}O_{3-\delta}$; (2) $La_{0.2}Ba_{0.8}Co_{0.2}Fe_{0.8}O_{3-\delta}$; (3) $La_{0.2}Ca_{0.8}Co_{0.2}Fe_{0.8}O_{3-\delta}$.

Figure 4 plots steady-state oxygen permeation flux for $La_{0.2}A_{0.8}Co_{0.2}Fe_{0.8}O_{3-\delta}$ (A = Sr, Ba, Ca) membranes at different temperatures. As shown in Figure 4, the oxygen fluxes become substantial above a critical temperature due to the order−disorder transition of the oxygen vacancy.[31] For $La_{0.2}A_{0.8}Co_{0.2}Fe_{0.8}O_{3-\delta}$ (A = Sr, Ba,) membranes, the critical temperatures are 750 °C and 800 °C, respectively. There is no obvious critical temperature for $La_{0.2}Ca_{0.8}Co_{0.2}Fe_{0.8}O_{3-\delta}$ membrane. The critical temperatures of perovskites also can be seen clearly from the TGA analysis in Figure 3 that around the temperatures the weights of samples changed rabidly. Figure 5 shows Arrhenius plots of the oxygen permeation flux data at temperatures higher than 800 °C. Regression analysis gives the following equation for

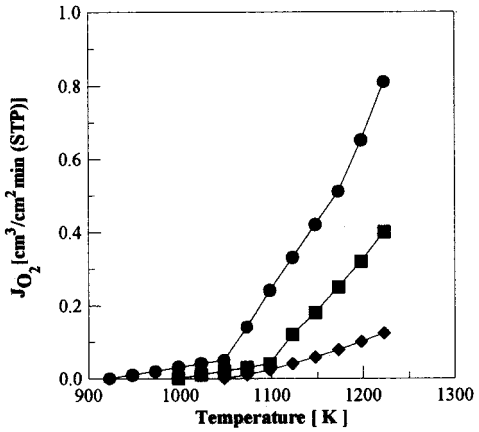

Figure 4. Temperature dependence of the oxygen permeability of the perovskite-type membranes at the partial pressure of 0.21/1 $\times$ 10^{-3} atm (helium flow rate: 30 mL/min): (●) $La_{0.2}Sr_{0.8}Co_{0.2}Fe_{0.8}O_{3-\delta}$; (■) $La_{0.2}Ba_{0.8}Co_{0.2}Fe_{0.8}O_{3-\delta}$; (◆) $La_{0.2}Ca_{0.8}Co_{0.2}Fe_{0.8}O_{3-\delta}$.

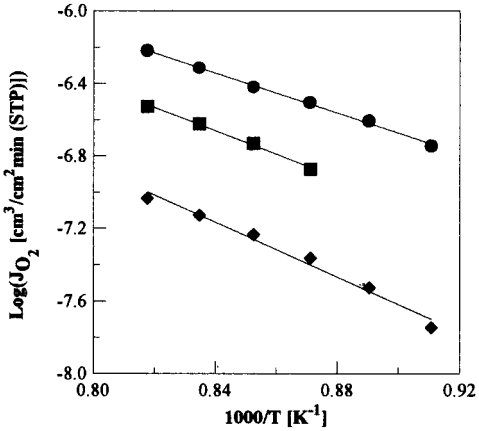

Figure 5. Arrhenius plot of the oxygen permeation flux of perovskite-type membranes at the partial pressure of 0.21/1 $\times$ 10^{-3} atm (helium flow rate, 30 mL/min): (●) $La_{0.2}Sr_{0.8}Co_{0.2}Fe_{0.8}O_{3-\delta}$; (■) $La_{0.2}Ba_{0.8}Co_{0.2}Fe_{0.8}O_{3-\delta}$; (◆) $La_{0.2}Ca_{0.8}Co_{0.2}$ $Fe_{0.8}O_{3-\delta}$.

the experimental relationship between J_{O_2} and T:

$$J_{O_2} = 0.021 \exp(-1.06 \times 10^5/RT) \quad (La_{0.2}Sr_{0.8}Co_{0.2}Fe_{0.8}O_{3-\delta}) \quad (6)$$

$$J_{O_2} = 0.058 \exp(-1.23 \times 10^5/RT) \quad (La_{0.2}Ba_{0.8}Co_{0.2}Fe_{0.8}O_{3-\delta}) \quad (7)$$

$$J_{O_2} = 0.015 \exp(-1.44 \times 10^5/RT) \quad (La_{0.2}Ca_{0.8}Co_{0.2}Fe_{0.8}O_{3-\delta}) \quad (8)$$

The activation energies for oxygen permeation of $La_{0.2}A_{0.8}Co_{0.2}Fe_{0.8}O_{3-\delta}$ (A = Sr, Ba, Ca) membranes are also listed in Table 3. The activation energies of $La_{0.2}A_{0.8}Co_{0.2}Fe_{0.8}O_{3-\delta}$ (A = Sr, Ba, Ca) perovskite-type membranes decrease in the order of Sr > Ba > Ca. Membranes with a lower oxygen permeation flux exhibit a higher activation energy for oxygen permeation.

3.3. Relationship between Crystallographic-Related Parameters and Oxygen Transport Rate. The perovskite crystallographic-related parameters associated with oxygen transport include the average metal−oxygen bond energy (ABE) of the perovskite lattice, the degree of openness, or "free volume" (V_F), and the critical radius (r_c).[35] Crystallographic lattice parameters obtained by X-ray powder diffraction were used to calculate free volume and critical radius. The effective radii for cations and anions were obtained from the literature.[36]

Table 4. The Relationships between Average Bonding Energy, Free Volume, and Critical Radius for Perovskite Membrane

membrane	average bond energy (kJ/mol)	free volume (Å^3)	critical radium (Å)	E_a (kJ/mol)
$La_{0.2}Sr_{0.8}Co_{0.2}Fe_{0.8}O_{3-\delta}$	286.46	13.765	0.79	106.04
$La_{0.2}Ba_{0.8}Co_{0.2}Fe_{0.8}O_{3-\delta}$	285.70	11.031	0.625	123.34
$La_{0.2}Ca_{0.8}Co_{0.2}Fe_{0.8}O_{3-\delta}$	288.14	13.17	0.732	143.99

For ideal cubic perovskite in which the A-site cations are 12-coordinated and the B-sites are 6-coordinated, the average perovskite bond energies are given by:[37]

$$ABE = \Delta(A - O) + \Delta(A' - O) + \Delta(B - O) + \Delta(B' - O) \quad (9)$$

where A′ and B′ are the substituting A-site cation and B-site cation, respectively. The equations applied to A′ and B′ are analogous to A and B. $\Delta(A - O)$ and $\Delta(B - O)$ are calculated by:

$$\Delta(A - O) = \frac{x_A}{12m}\left(\Delta H_{A_mO_n} - m\Delta H_A - \frac{n}{2} D_{O_2}\right) \quad (10)$$

$$\Delta(B - O) = \frac{x_B}{6m}\left(\Delta H_{B_mO_n} - m\Delta H_B - \frac{n}{2} D_{O_2}\right) \quad (11)$$

where x_A and x_B are the molar fraction of metals A and B, respectively; $\Delta H_{A_mO_n}$ and $\Delta H_{B_mO_n}$ are the heats of formation of A_mO_n and B_mO_n at 298 K, respectively[38,39]; ΔH_A and ΔH_B are the heats of sublimation of metals A and B at 298 K, respectively, and D_{O_2} is the oxygen dissociation energy (500.2 kJ/mol).

The critical radius represents the saddle point formed by two A-site and one B-site cations through which the mobile anion must pass.[35] For the calculation of critical radius, r_c, the following equation can be used:

$$r_c = \frac{\frac{3}{4}a_0^2 - r_A^2 + r_B^2 - \sqrt{2}a_0 r_b}{2r_A - 2r_B + \sqrt{2}a_0} \quad (12)$$

where r_A and r_B are the radii of ion A and B, respectively, and a_0 is the lattice parameter for the cubic structure.

Free volume (V_F) of the lattice obtained by subtracting the ionic volumes of cations and O^{2-} in the unit cell from the overall unit cell volume,

$$V_F = a_0^3 - \frac{4}{3}\pi(r_A^3 + r_B^3 + (3 - \delta)r_O^2) \quad (13)$$

where r_O is the radius of O^{2-}.

The calculated ABE, critical radius (r_c), and free volume (V_F) of the $La_{0.2}A_{0.8}Co_{0.2}Fe_{0.8}O_{3-\delta}$ (A = Sr, Ba, Ca) perovskite lattice at room temperature are listed in Table 4. In general, the higher the ABE, the higher the activation energy for perovskite, because the ABE

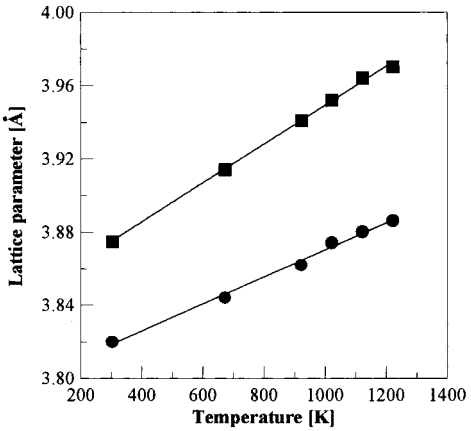

Figure 6. Temperature dependence of lattice parameter of perovskite-type membranes: (●) $La_{0.2}Sr_{0.8}Co_{0.2}Fe_{0.8}O_{3-\delta}$; (■) $La_{0.2}Ba_{0.8}Co_{0.2}Fe_{0.8}O_{3-\delta}$.

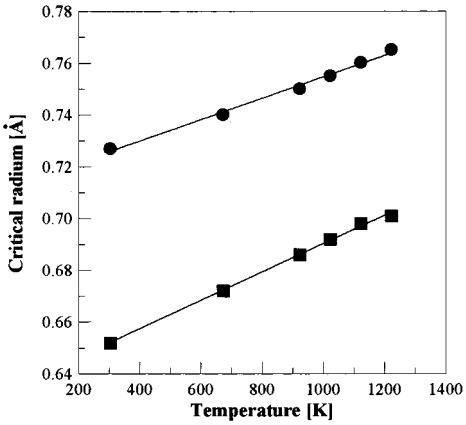

Figure 7. Temperature dependence of critical radius of perovskite-type membranes: (●) $La_{0.2}Sr_{0.8}Co_{0.2}Fe_{0.8}O_{3-\delta}$; (■) $La_{0.2}Ba_{0.8}Co_{0.2}Fe_{0.8}O_{3-\delta}$.

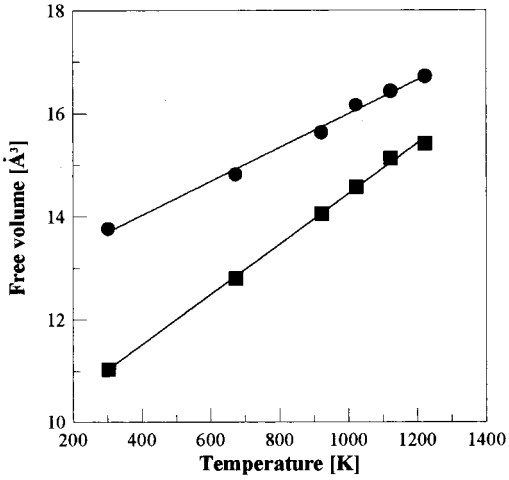

Figure 8. Temperature dependence of free volume of perovskite-type membranes: (●) $La_{0.2}Sr_{0.8}Co_{0.2}Fe_{0.8}O_{3-\delta}$; (■) $La_{0.2}Ba_{0.8}Co_{0.2}Fe_{0.8}O_{3-\delta}$.

may be related to the dissociation of the surface oxygen as well as to the oxygen transport in the bulk. On the other hand, the higher the free volume, the lower the activation energy for perovskite, because the free volume provides activation volume for the transport of ions. Two factors should be thought about at the same time to determine the activation energy and oxygen permeability for perovskite. The Ca-substitution compound had the larger free volume, but had the highest ABE, which might eliminate the positive effect of the larger free volume on oxygen transport, so the activation energy is the highest. The Ba-substitution compound has the lowest ABE, but has the smallest free volume, which might eliminate the lowest ABE, so the activation energy is also high. The Sr-substitution compound has the lower ABE and the highest free volume, so the activation energy is the lowest. Also $La_{0.2}Sr_{0.8}Co_{0.2}Fe_{0.8}O_{3-\delta}$ perovskite-type oxide has the largest critical radius, so the diffusivity and oxygen permeation flux is the highest.

The difference in oxygen permeation fluxes among the work of Teraoka et al.,[27] Tai et al.,[13] Stevenson et al.[28] and our groups is that the former two groups reported a lower oxygen permeation flux for $La_{0.2}Sr_{0.8}Co_{0.2}Fe_{0.8}O_{3-\delta}$ than $La_{0.2}Ba_{0.8}Co_{0.2}Fe_{0.8}O_{3-\delta}$, and the latter two groups reported the opposite result. The free volume and critical radius data at room temperature were used in the work of Tsai et al.[13] and earlier in this work to explain the oxygen permeation rate. To examine more accurately the effects of the crystallographic parameters on the oxygen transport properties, it is more important to measure the values of these two parameters at high temperatures.

Crystallographic lattice parameters were obtained by X-ray powder diffraction at high temperatures, assuming that iron radii do not change as the temperature increases. Figure 6 shows temperature dependence of lattice parameter of perovskite-type membranes. Dependence of the unit cell volume on the oxygen content of the sample (by TGA data) has been established by comparing the lattice parameters (by XRD data). The results show that $La_{0.2}Sr_{0.8}Co_{0.2}Fe_{0.8}O_{3-\delta}$ and $La_{0.2}Ba_{0.8}Co_{0.2}Fe_{0.8}O_{3-\delta}$ perovskite-type membranes expand as oxygen is removed. Figures 7 and 8 show temperature dependence of critical radius and free volume of perovskite-type membranes. It can be seen from the figures that critical radius and free volume of $La_{0.2}Sr_{0.8}Co_{0.2}Fe_{0.8}O_{3-\delta}$ perovskite-type membrane are still higher than those of $La_{0.2}Ba_{0.8}Co_{0.2}Fe_{0.8}O_{3-\delta}$ membrane at high temperatures. Thus the conclusion obtained earlier based on the room-temperature, crystallographic–related parameters is still valid.

3.4. Chemical Stability. The high-temperature phase stability of $LaFeO_3$ and $LaCoO_3$, has been studied by Nakamura et al.[40] At 1473 K, undoped $LaFeO_3$ was stable in the perovskite phase above a critical oxygen activity of 10−13.5. The dissociation of $LaFeO_3$ (into La_2O_3 and Fe) occurred in one simple step. On the other hand, $LaCoO_3$ was much less stable under reducing atmosphere. It transformed to La_2O_3 and Co after formation of several intermediate phases. In the study of Tai et al.[41] the thermochemical properties of $La_{1-x}Sr_xCo_{0.2}Fe_{0.8}O_{3-\delta}$ (x = 0, 0.2, 0.4) appear to follow the boundaries set between the two end members, $LaFeO_3$ and $LaCoO_3$, but the electrical properties are closer to those of $LaFeO_3$. The Sr content ($x < 0.4$) does not seem to have a significant effect on the temperature phase stability.

Because the oxygen permeation flux of $La_{0.2}Ca_{0.8}Co_{0.2}Fe_{0.8}O_{3-\delta}$ membrane is very low, here we only analyze the phase stability of two more oxygen-permeable $La_{0.2}Sr_{0.8}Co_{0.2}Fe_{0.8}O_{3-\delta}$ and $La_{0.2}Sr_{0.8}Co_{0.2}Fe_{0.8}O_{3-\delta}$ membranes. X-ray diffraction patterns of $La_{0.2}Sr_{0.8}Co_{0.2}Fe_{0.8}O_{3-\delta}$ and $La_{0.2}Ba_{0.8}Co_{0.2}Fe_{0.8}O_{3-\delta}$ powders crashed by the membranes at various temperatures in air are shown in Figures 9 and 10. As shown, both $La_{0.2}Sr_{0.8}Co_{0.2}Fe_{0.8}O_{3-\delta}$ and $La_{0.2}Ba_{0.8}Co_{0.2}Fe_{0.8}O_{3-\delta}$ membranes are

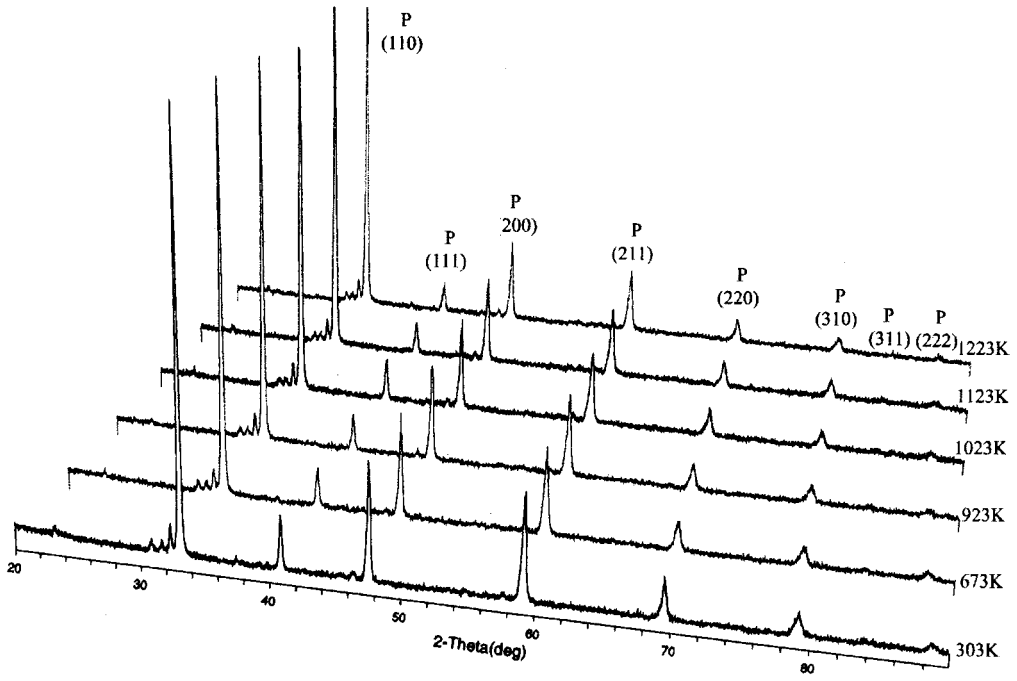

Figure 9. X-ray diffraction patterns of the $La_{0.2}Sr_{0.8}Co_{0.2}Fe_{0.8}O_{3-\delta}$ membrane at various temperatures in air: (P) Perovskite.

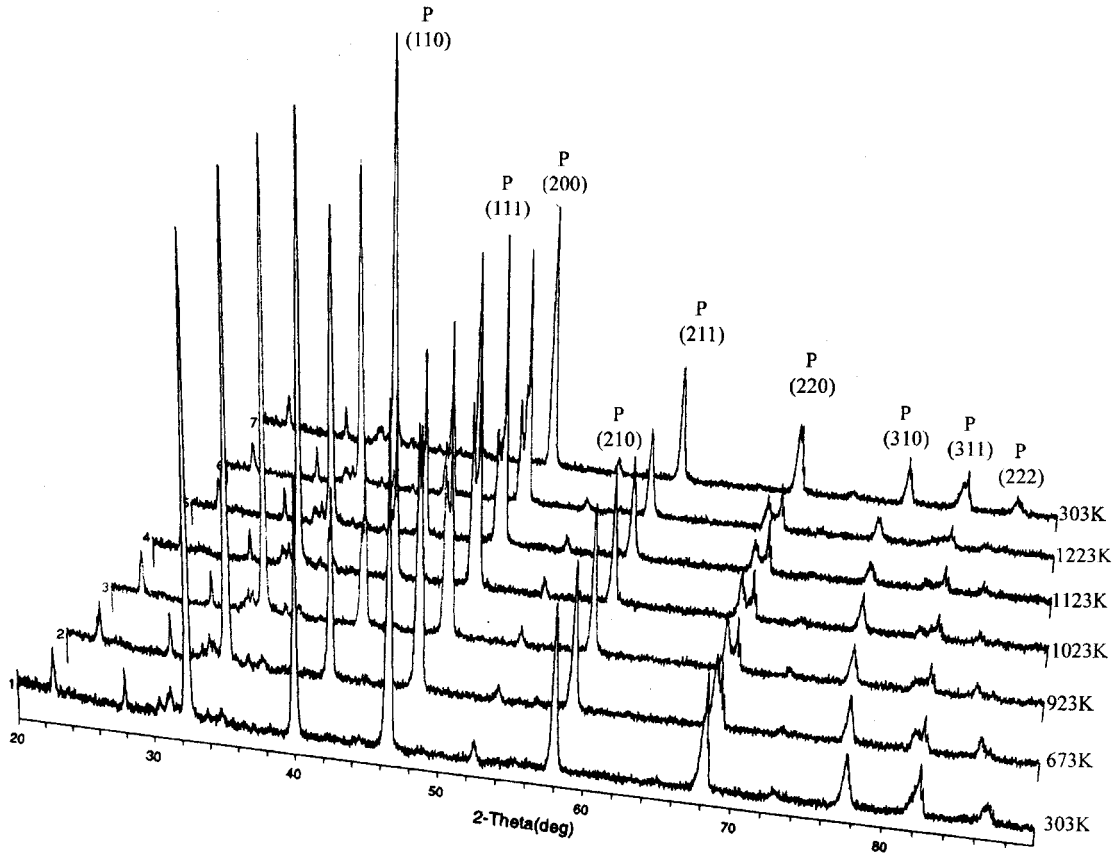

Figure 10. X-ray diffraction patterns of the $La_{0.2}Ba_{0.8}Co_{0.2}Fe_{0.8}O_{3-\delta}$ membrane at various temperatures in air: (P) Perovskite.

very stable at temperatures up to 1223 K in oxygen-rich atmosphere (air).

X-ray diffraction patterns of $La_{0.2}Sr_{0.8}Co_{0.2}Fe_{0.8}O_{3-\delta}$ and $La_{0.2}Ba_{0.8}Co_{0.2}Fe_{0.8}O_{3-\delta}$ powders crashed by membranes at various temperatures in argon are shown in Figures 11 and 12. Phases of the two membranes at high temperatures are listed in Table 5. For $La_{0.2}Sr_{0.8}Co_{0.2}Fe_{0.8}O_{3-\delta}$ membrane, at the temperatures higher than 1023 K, new XRD peaks (La_2O_3, SrO, CoO, Fe) appeared near the XRD peaks of the perovskite phase. This indicates that part of the perovskite phase has been transformed to La_2O_3, SrO, CoO, Fe. Compared with those in the air (Figure 9), the XRD peaks of the $La_{0.2}Sr_{0.8}Co_{0.2}Fe_{0.8}O_{3-\delta}$ perovskite phase become less intensive and broader, indicating a decrease in the crystallite size of the perovskite phase. However, the XRD patterns and peak broadness of $La_{0.2}Ba_{0.8}Co_{0.2}Fe_{0.8}O_{3-\delta}$ membrane after exposure to Ar at various

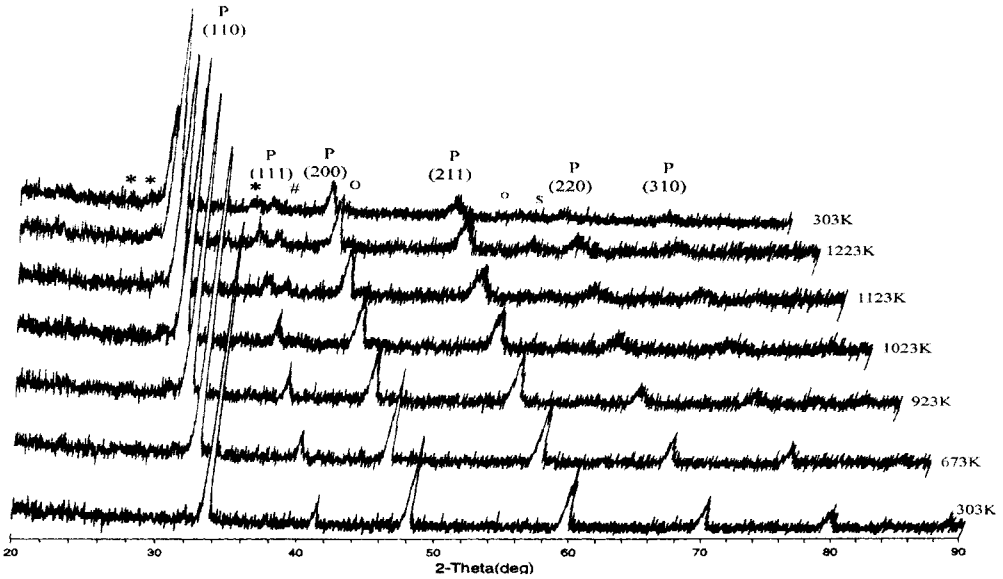

Figure 11. X-ray diffraction patterns of the $La_{0.2}Sr_{0.8}Co_{0.2}Fe_{0.8}O_{3-\delta}$ membrane at various temperatures in argon: (P) Perovskite; (∗) La_2O_3; (#) CoO; (○) SrO; ($) Fe.

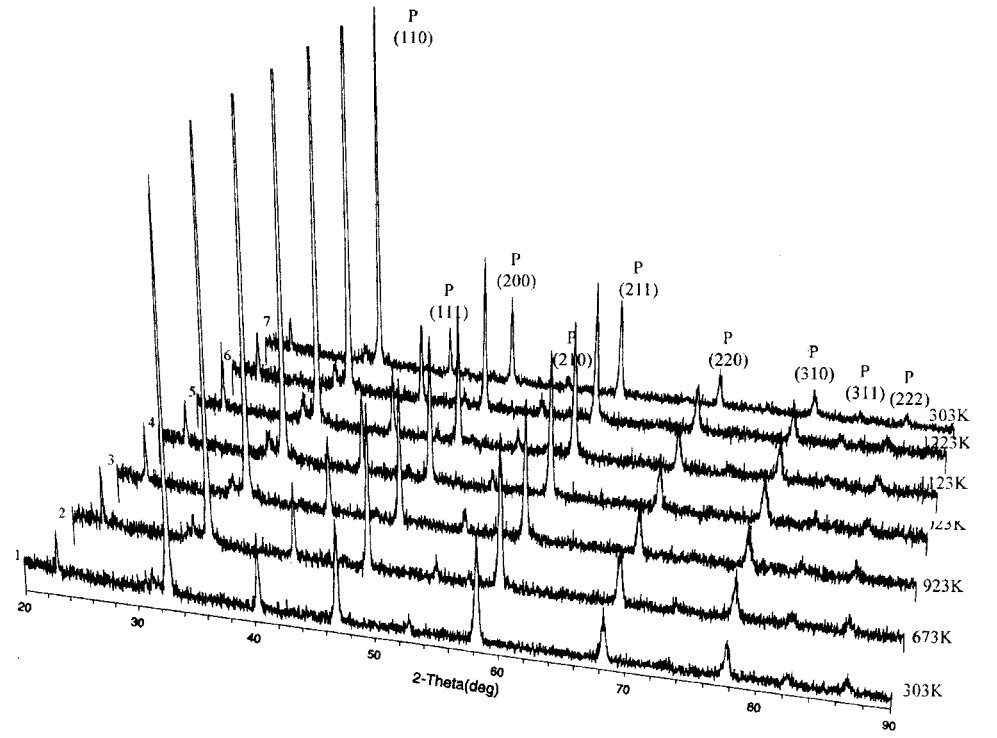

Figure 12. X-ray diffraction patterns of the $La_{0.2}Ba_{0.8}Co_{0.2}Fe_{0.8}O_{3-\delta}$ membrane at various temperatures in argon: (P) Perovskite.

Table 5. Phases of Membranes at High Temperature in Argon

membrane	temperature (K)	phases
$La_{0.2}Sr_{0.8}Co_{0.2}Fe_{0.8}O_{3-\delta}$	<923	perovskite
	>923	perovskite, SrO, La_2O_3, CoO, Fe
$La_{0.2}Ba_{0.8}Co_{0.2}Fe_{0.8}O_{3-\delta}$	<923	perovskite
	>923	perovskite

temperatures remain essentially the same. No new phases are formed in this membrane after these treatments. This shows that $La_{0.2}Ba_{0.8}Co_{0.2}Fe_{0.8}O_{3-\delta}$ membrane is more stable than $La_{0.2}Sr_{0.8}Co_{0.2}Fe_{0.8}O_{3-\delta}$ membrane at high temperature and low oxygen partial pressure.

4. Conclusions

$La_{0.2}A_{0.8}Co_{0.2}Fe_{0.8}O_{3-\delta}$ (A = Sr, Ba, Ca) perovskite-type membranes were prepared by the solid-state method with desired properties and high oxygen permeation flux. The oxygen vacancy diffusivity and concentration gradient could be calculated from the oxgyen unsteady-state and steady-state oxygen permeation data. They decrease in the order of Sr > Ba > Ca for these three perovskite-type membranes. The activation energies for oxygen permeation of $La_{0.2}A_{0.8}Co_{0.2}Fe_{0.8}O_{3-\delta}$ (A = Sr, Ba, Ca) membranes are 106.4, 123.3, 144.0 kJ/mol, respectively.

Sr-substitution compound has the highest oxygen permeation fluxes because of the lower average bond energy, highest free volume, and largest critical radius.

At high temperatures, the critical radius and free volume of $La_{0.2}Sr_{0.8}Co_{0.2}Fe_{0.8}O_{3-\delta}$ perovskite-type membranes are higher than those of $La_{0.2}Ba_{0.8}Co_{0.2}Fe_{0.8}O_{3-\delta}$ perovskite-type membranes, which confirms the conclusion mentioned above based on room-temperature crystallographic data.

$La_{0.2}Sr_{0.8}Co_{0.2}Fe_{0.8}O_{3-\delta}$ membrane is not stable at high temperature and low oxygen partial pressure atmosphere. Under these conditions part of $La_{0.2}Sr_{0.8}Co_{0.2}Fe_{0.8}O_{3-\delta}$ was transformed to La_2O_3, SrO, Co, Fe, and the crystallite size of the perovskite phase decreased. These changes were not observed for $La_{0.2}Ba_{0.8}Co_{0.2}Fe_{0.8}O_{3-\delta}$ membrane under the same conditions, indicating better stability of this membrane at high temperature and in low oxygen partial pressure.

Acknowledgment

This work was supported by the National Advanced Materials Committee of China (NAMCC, no. 715-006-0120), and the National Natural Science Foundation of China (NNSFC, no. 59789201). We also would like to acknowledge the support of the U. S. Department of Energy, Basic Energy Sciences, Division of Materials Sciences (USDOE/BES/DMS) on high temperature X-ray diffraction analysis.

Nomenclature

a_0 = lattice parameter for the cubic structure (Å)
r_A = radius of ion A (Å)
r_B = radius of ion B (Å)
r_O = radius of O^{2-} (Å)
r_c = critical radius of the perovskite-type oxide (Å)
t = time (h)
t_{equil} = equilibration time (min)
ABE = average metal−oxygen bond energy (kJ/mol)
C_v = oxygen vacancy concentration (mol/cm^3)
C_v' = oxygen vacancy concentration of the oxygen upstream (mol/cm^3)
C_v'' = oxygen vacancy concentration of the oxygen downstream (mol/cm^3)
D_{O_2} = oxygen dissociation energy (kJ/mol)
D_v = oxygen diffusivity (cm^2/s)
E_a = activation energy for diffusion of oxygen (kJ/mol)
J_{O_2} = oxygen permeation flue (mL/cm^2 min)
L = the membrane thickness (cm)
R = gas constant
T= temperature (K)
V_F = free volume of the lattice (Å^3)
V_m = molar volume of the membrane (Å^3)
δ = nonstoichiometry of oxygen in mole formula
δ_{N_2} = δ at N_2 atmosphere
δ_{air} = δ at air atmosphere
ΔC_v = the change of oxygen vacancy concentration (mol/cm^3)
ΔH_A = heat of sublimation of metal A at 298 K (kJ/mol)
$\Delta H_{A_mO_n}$ = heat of formation of A_mO_n at 298 K (kJ/mol)
H_{B_n} = heat of sublimation of metal B at 298 K (kJ/mol)
$\Delta H_{B_mO_n}$ = heat of formation of B_mO_n at 298 K (kJ/mol)

Literature Cited

(1) Carolan, M. F.; Dyer, P. N.; LaBar Sr., J. M.; Thorogood, R. M. Process for Recovering Oxygen from Gaseous Mixture Containing Water or Carbon Dioxide Which Process Employs Ion Transport Membranes. U.S. Patent 5,261,932, 1993.

(2) Carolan, M. F.; Dyer, P. N.; Fine, S. M.; LaBar Sr., J. M.; Thorogood, R. M. Process for Recovering Oxygen from Gaseous Mixture Containing Water or Carbon Dioxide Which Process Employs Barium-Containing Ion Transport Membranes. U.S. Patent 5,269,822, 1993.

(3) Carolan, M. F.; Dyer, P. N.; LaBar Sr., J. M.; Thorogood, R. M. Process for Restoring Permeance of and Recovering Oxygen from Gaseous Mixture Containing Water or Carbon Dioxide Which Process Employs Barium-Containing Ion Transport Membranes. U.S. Patent 5,240,437, 1993.

(4) Liu, M.; Joshi, A. V.; Shen, Y.; Krist, K. Mixed Ionic-Electronic Conductors for Oxygen Separation and Electrocatalysis. U.S. Patent 5,273,628, 1993.

(5) Hazbun, E. A. Ceramic Membrane and Use Thereof for Hydrocarbon Conversion. U.S. Patent 4,827,071, 1989.

(6) ten Elshof, J. E.; Van Hassel, B. A.; Bouwmeester, H. J. M. Activation of Methane Using Solid Oxide Membrane. *Catal. Today* **1995**, *25*, 397.

(7) ten Elshof, J. E.; Bouwmeester, H. J. M.; Verweij, H. Oxidative Coupling of Methane in a Mixed-Conducting Perovskite Membrane Reactor. *Appl. Catal. A* **1995**, *130*, 195.

(8) Nozaki, T.; Fujimoto, K. Oxide Ion Transport for Selective Oxidative Coupling of Methane with New Membrane Reactor. *AIChE J.* **1994**, *40*, 870.

(9) Wang, W.; Lin, Y. S. Analysis of Oxidative Coupling in Dense Oxide Membrane Reactors. *J. Membr. Sci.* **1995**, *103*, 219.

(10) Lin, Y. S.; Zeng, Y. Catalytic Properties of Oxygen Semipermeable Perovskite Type Ceramic Membrane Materials for Oxidative Coupling of Methane. *J. Catal.* **1996**, *164*, 220.

(11) Jin, W.; Li, S.; Huang, P.; Xu, N.; Shi, J.; Lin, Y. S. Tubular Lanthanum Cobaltite Perovskite Type Membrane for Partial Oxidation of Methane to Syngas. *J. Membr. Sci.*, accepted for publication.

(12) Tsai, C.-Y.; Dixon, A. G.; Moser, W. R.; Ma, Y. H. Dense Perovskite Membrane Reactors for the Partial Oxidation of Methane to Syngas. *AIChE J.* **1997**, *43*, 2741.

(13) Tsai, C. Y.; Dixon, A. G.; Ma, Y. H.; Moser, W. R.; Pascucci, M. R. Dense Perovskite, $La_{1-x}A'_xFe_{1-y}Co_yO_{3-\delta}$ (A′=Ba, Sr, Ca), Membrane Synthesis, Application, and Characterization. *J. Am. Ceram. Soc.* **1998**, *81*, 1437.

(14) Pei, S.; Kleefisch, M. S.; Kobylinski, T. P.; Faber, K.; Udovich, C. A.; Zhang-Mccoy, V.; Dabrowski, B.; Balachandran, U.; Mieville, R. L.; Poeppel, R. B. Failure Mechanisms of Ceramic Membrane Reactors in Partial Oxidation of Membrane to Synthesis Gas. *Catal. Lett.* **1995**, *30*, 201.

(15) Balachandran, U.; Dusk, J. T.; Mieville, R. L.; Poeppel, R. B.; Kleefisch, M. S.; Pei, S.; Kobylinski, T. P.; Udovich, C. A.; Bose, A. C. Dense Ceramic Membranes for Partial Oxidation of Methane to Syngas. *Appl. Catal. A* **1995**, *133*, 19.

(16) Balachandran, U.; Dusk, J. T.; Maiya, P. S.; Ma, B.; Mieville, R. L.; Kleefisch, M. S.; Udovich, C. A. Ceramic Membrane Reactor for Converting Methane to Syngas. *Catal. Today* **1997**, *36*, 265.

(17) Gur, T. M.; Belzner, A.; Huggins, R. A. A New Class of Oxygen Selective Chemically Driven Nonporous Ceramic Membrane. Part I. A-Site Doped Perovskites. *J. Membr. Sci.* **1992**, *75*, 151.

(18) Itoh, N.; Kato, T.; Uchida, K.; Haraya, K. Preparation of Pore-Free Disk of $La_{1-x}Sr_xCoO_3$ Mixed Conductor and Its Oxygen Permeability. *J. Membr. Sci.* **1994**, *92*, 239.

(19) van Hassel, B. A.; Kawada, T.; Sakai, N.; Yokokana, H.; Dokiya, M. Oxygen Permeation Modeling of $La_{1-y}Ca_yCrO_{3-\delta}$. *Solid State Ionics* **1993**, *61*, 41.

(20) van Hassel, B. A.; Kawada, T.; Sakai, N.; Yokokana, H.; Bouwmeester, H. J. M. Oxygen Permeation Modeling of Perovskites. *Solid State Ionics* **1993**, *66*, 295.

(21) van Hassel, B. A.; ten Elshof, J. E.; Bouwmeester, H. J. M. Oxygen Permeation Flux Through $La_{1-y}Sr_yFeO_{3-\delta}$ Limited by Carbon Monoxide Oxidation Rate. *Appl. Catal. A* **1994**, *119*, 279.

(22) Kawada, T.; Horita, T.; Sakai, N.; Yokokawa, H.; Dokiya, M. Experimental Determination of Oxygen Permeation Flux through Bulk and Grain Boundary of $La_{0.7}Ca_{0.3}CrO_3$. *Solid State Ionics* **1995**, *79*, 201.

(23) Chen, C. H.; Bouwmeester, H. J. M.; van Doorn, R. H. E.; Kruidhof, H.; Burggraaf, A. J. Oxygen Permeation of $La_{0.3}Sr_{0.7}CoO_{3-\delta}$. *Solid State Ionics* **1997**, *98*, 7.

(24) ten Elshof, J. E.; Bouwmeester, H. J. M.; Verweij, H. Oxygen Transport through $La_{1-x}Sr_xFeO_{3-\delta}$ Membrane. I. Permeation in Air/He Gradients. *Solid State Ionics* **1995**, *81*, 97.

(25) Qiu, L.; Lee, T. H.; Liu, L.-M.; Yang, Y. L.; Jacobson, A. J. Oxygen Permeation Studies of $SrCo_{0.8}Fe_{0.2}O_{3-\delta}$. *Solid State Ionics* **1995**, *76*, 321.

(26) Kharton, V. V.; Naumovich, E. N.; Nikolaev, A. V. Materials of High-Temperature Electrochemical Oxygen Membranes. *J. Membr. Sci.* **1996**, *111*, 149.

(27) Teraoka, Y.; Nobunaga, T.; Yamazoe, N. Effect of Cation Substitution on the Oxygen Semipermeability of Perovskite Oxides. *Chem. Lett.* **1988**, 503.

(28) Stevenson, J. W.; Armstrong, T. R.; Carmeim, R. D.; Pederson, L. R.; Weber, L. R. Electrochemical Properties of Mixed Conducting Perovskites $La_{1-x}M_xCo_{1-y}Fe_yO_{3-\delta}$ (M = Sr, Ba, Ca). *J. Electrochem. Soc.* **1996**, *143*, 2722.

(29) Teraoka, Y.; Zhang, H. M.; Furukawa, S.; Yamazoe, N. Oxygen Permeation through Perovskite-Type Oxides. *Chem. Lett.* **1985**, 1743.

(30) Kruidhof, H.; Bouwmeester, H. J. M.; Doom, R. H. E. V.; Burggraaf, A. J. Influence of Order−Disorder Transitions on Oxygen Permeability Through Selected Nonstoichiometric Perovskite-Type Oxides. *Solid State Ionics* **1993**, *63*−*65*, 816.

(31) Zeng, Y.; Lin, Y. S.; Swartz, S. L. Perovskite Type Ceramic Membranes: Synthesis, Oxygen Permeation and Membrane Reactor Performance for Oxidative Coupling of Methane. *J. Membr. Sci.* **1998**, *150*, 687.

(32) Xu, S. J.; Thomson, W. J. Stability of $La_{0.6}Sr_{0.4}Co_{0.2}Fe_{0.8}O_{3-\delta}$ Perovskite Membrane in Reducing and Nonreducing Environments. *Ind. Eng. Chem. Res.* **1998**, *37*, 1290.

(33) Li, S.; Jin, W.; Huang, P.; Xu, N.; Shi, J. Perovskite-related ZrO_2-doped $SrCo_{0.4}Fe_{0.6}O_{3-\delta}$ membrane for oxygen permeation. *AIChE J.* **1999**, *45*, 276.

(34) Li, S.; Jin, W.; Huang, P.; Xu, N.; Shi, J.; Lin, Y. S. Tubular Lanthanum Cobaltite Perovskite Type Membrane for Oxygen Permeation. *J. Membr. Sci.*, accepted for publication.

(35) Sammells, A. F.; Cook, R. L.; White, J. H.; Osborne, J. J.; MacDuff, R. C. Rational Selection of Advanced Solid Electrolytes for Intermediate Temperature Fuel Cells. *Solid State Ionics* **1992**, *52*, 111.

(36) Richerson, D. W. *Modern Ceramic Engineering Properties, Processing, and Use in Design*, 2nd ed.; 1992; p. 378.

(37) Voorhoeve, R. J. H.; Remeika, J. P.; Trimble, L. E. Defect Chemistry and Catalysis in Oxidation and Reduction over Perovskite-Type Oxides. *Ann. N. Y. Acad. Sci.* **1976**, *272*, 3.

(38) Kubaschewski, O.; Evans, E. LL.; Alcock, C. B. *Metallurgical Thermochemistry*, 4th ed.; 1967.

(39) Tsai, C. Y. Perovskite Dense Membrane Reactors for the Partial Oxidation of Methane to Syngas. Ph.D. Dissertation, Worcester Polytechnic Institute, Worcester, MA, 1996.

(40) Nakamura, R.; Petzow, G.; Gauckler, L. J. Stability of the Perovskite Phase LaBO3 (B═V, Cr, Mn, Fe, Co, Ni) in a Reducing Atmosphere. I. Experimental Results. *Mater. Res. Bull.* **1979**, *14*, 674.

(41) Tai, L −W.; Nasrallan, M. M.; Anderson, H. U. Thermochemical Stability, Electrical Conductivity, and Seebeck Coefficient of Sr-Doped $LaCo_{0.2}Fe_{0.8}O_{3-\delta}$. *J. Solid State Chem.* **1995**, *118*, 117.

Received for review January 4, 1999
Revised manuscript received May 21, 1999
Accepted May 21, 1999

IE9900014